INSTITUTE OF PHYSICS PUBLISHING NANOTECHNOLOGY

Nanotechnology **14** (2003) 117–122 PII: S0957-4484(03)54437-3

Ballistic nanodevices for terahertz data processing: Monte Carlo simulations

J Mateos[1], B G Vasallo[1], D Pardo[1], T González[1], J S Galloo[2], Y Roelens[2], S Bollaert[2] and A Cappy[2]

[1] Universidad de Salamanca, Plaza de la Merced s/n, 37008 Salamanca, Spain
[2] Institut d'Electronique, de Microélectronique et de Nanotechnologie UMR CNRS no 9929, Département Hyperfréquences et Semiconducteurs, BP 69, 59652 Villeneuve D'Ascq Cédex, France

E-mail: javierm@usal.es (J Mateos)

Received 8 October 2002, in final form 10 December 2002
Published 10 January 2003
Online at stacks.iop.org/Nano/14/117

Abstract
By using a semi-classical two-dimensional Monte Carlo simulation, simple devices (T-branch junctions (TBJs) and rectifying diodes) based on AlInAs/InGaAs ballistic channels are analysed. Initially, the model is validated by means of Hall-effect measurements of mobility and electron concentration in long (diffusive) channels. Then, quasi-ballistic transport at room temperature is confirmed in a 100 nm channel. Our simulations qualitatively reproduce the experimental results of electric potential measured in a TBJ appearing as a result of electron ballistic transport, and in close relation with the presence of space charge inside the structure. As examples of devices exploiting the ballistic transport of electrons, preliminary simulations of a multiplexor/demultiplexor and a rectifying diode are presented, demonstrating their capability for terahertz operation.

(Some figures in this article are in colour only in the electronic version)

1. Introduction

Recent works have shown ballistic effects up to room temperature in InGaAs channels thanks to the long mean free path of electrons, still larger than 100 nm at room temperature [1]. Consequently, the fabrication of basic devices using ballistic effects can be envisaged, for example, a ballistic rectifier or a multiplexor/demultiplexor (MUX/DEMUX) for data processing at ultra-high bit rate. InGaAs-based ballistic devices are compatible with advanced InP HEMT technology; indeed AlInAs/InGaAs HEMTs nowadays operate in the millimetre and infrared frequency range. Thus, the integration of ballistic devices with HEMTs in order to benefit from their complementary advantages and reach the terahertz (THz) regime appears feasible in the near future.

The first step in the design of ballistic structures is the determination of their optimal geometry. At this level, simulation tools constitute a valuable alternative to the expensive and time-consuming test-and-error procedure. In this contribution we present a microscopic analysis, based on Monte Carlo (MC) simulations, of the transport properties of several structures based on AlInAs/InGaAs ballistic channels specially designed to be applied in electronic devices for THz data processing.

In section 2 the details about the MC model and the simulated structures will be given. Then in section 3 results from the simulation of different kind of structures are shown: firstly, real AlInAs/GaInAs channels, with the layer structure typically used in the fabrication of HEMTs, considering a sample of length L between two ohmic contacts. Then, simulations of InGaAs channels with different geometries have been performed: the results of T-branch junctions (TBJs), a MUX/DEMUX and a ballistic rectifier are presented.

2. Monte Carlo model

We will make use of a semi-classical MC model self-consistently coupled with a 2D Poisson solver. The transport model locally takes into account the effect of degeneracy and electron heating by using the rejection technique and the self-consistent calculation of the local electronic temperature and Fermi level [2]. The surface charges appearing on

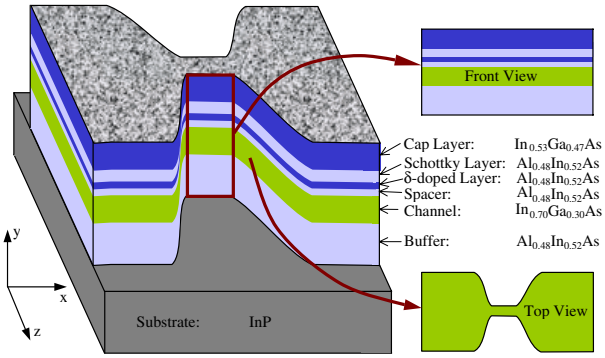

Figure 1. 3D geometry and layer structure of the ballistic channels and scheme of the 2D FV and TV MC simulations.

the semiconductors in contact with the dielectrics are also considered in the model [3]. The validity of this approach has been checked in previous works by means of the comparison with experimental results of static characteristics, small signal behaviour and noise performance of a 0.1 μm gate AlInAs/GaInAs lattice-matched HEMT (InP based) [3, 4]. Since contact injection is a critical point when dealing with ballistic transport, the velocity distribution and time statistics of injected carriers will be accurately modelled [5].

The main features of the ballistic channels that will be simulated are shown in figure 1, where the geometry will be defined in the fabrication process by a typical mesa etching. The real layer structure fabricated by molecular beam epitaxy consists of an InP substrate, a 200 nm $Al_{0.48}In_{0.52}As$ buffer followed by a 15 nm thick $In_{0.7}Ga_{0.3}As$ strained channel, three layers of $Al_{0.48}In_{0.52}As$ (a 5 nm spacer, a δ-doped layer and a 10 nm Schottky layer) and finally a 15 nm thick $In_{0.53}Ga_{0.47}As$ cap layer ($N_D = 6 \times 10^{18}$ cm^{-3}). Layers with two different δ-dopings have been fabricated, 4 and 5×10^{12} cm^{-2}, they will be modelled as a 4 nm layer doped at 10^{19} cm^{-3} for the $\delta = 4 \times 10^{12}$ cm^{-2} and 1.25×10^{19} cm^{-3} for the $\delta = 5 \times 10^{12}$ cm^{-2} (moreover, a structure with $\delta = 6 \times 10^{12}$ cm^{-2} will be also simulated using $N_D = 1.5 \times 10^{19}$ cm^{-3}). To account for the thickness of the δ-doped layer while keeping the overall dimensions, the thickness of the spacer and Schottky layer are set to 3 and 8 nm, respectively.

For the correct modelling of these devices a 3D simulation would be necessary in order to take into account the effect of the lateral surface charges and the real geometry of the structure. However, for the moment only a 2D MC model has been developed and some simplifications and assumptions must be made. Indeed, two different types of 2D simulations will be performed, front-view (FV) and top-view (TV). Within the FV simulations the layer structure will be taken into account, but the device in the z dimension is considered to be homogeneous. This kind of simulation will be useful for simple structures, like homogeneous channels, and will provide the concentration of carriers in each layer. On the other hand, to account for the top geometry of more complicated devices (such as TBJ or ballistic diodes) TV simulations will be made. They are made on the xy plane and therefore the real layer structure is not included and only the channel will be simulated. In order to account for the fixed charges of the whole layer structure a net doping is assigned to the channel, but impurity scattering is switched off. In this way, the electron transport through the undoped channel

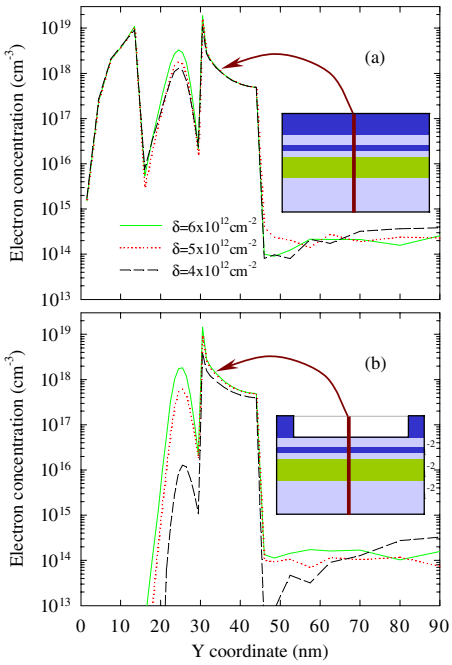

Figure 2. Vertical profiles of electron concentration in the structures (a) without recess and (b) with recess, and δ-dopings of 4×10^{12}, 5×10^{12} and 6×10^{12} cm^{-2}.

is well reproduced, since this is a 'virtual' doping associated to the charges of the cap and δ-doped layers. However, this model is not completely correct and the values of two important parameters must be correctly chosen to improve its accuracy: the background doping in the channel and the lateral surface charges.

3. Results

3.1. Ballistic channels

Initially, the validity of the simulation tools is checked by comparison of the numerical results with experimental Hall-effect measurements of carrier concentration and mobility of the two fabricated layers ($\delta = 4 \times 10^{12}$ and 5×10^{12} cm^{-2}). The concentration profiles obtained from the MC simulation of the layer structure (FV simulation) are shown in figure 2(a). By adjusting the surface charge at the cap layer to a value of $\sigma_{cap}/q = 4.7 \times 10^{12}$ cm^{-2}, we have obtained a good agreement with the measured values of Hall density in both layers.

For improving the ballistic character of the transport, impurity scattering will be diminished by allowing the transport just through the InGaAs channel. For this sake, recessed channels (the cap layer is removed) will be used. Again, by using Hall-effect measurements of the recessed structures the value of the surface charge at the bottom of the recess (free AlInAs interface) has also been determined, $\sigma_{rec}/q = 2.8 \times 10^{12}$ cm^{-2}. In figure 2(b) we can observe that choosing $\delta = 4 \times 10^{12}$ cm^{-2} the channel population is not degraded while avoiding a (non-ballistic) parasitic channel in the delta-doped AlInAs layer thus minimizing impurity scattering and improving the ballistic character of electron transport. However, we have appreciated that the channel mobility obtained with MC simulations overestimates the

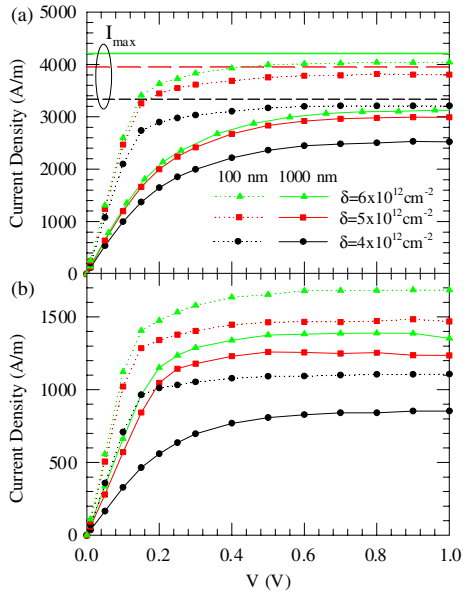

Figure 3. Current density versus applied voltage for the (a) non-recessed and (b) recessed channels, with $L = 100$ nm (dotted curves) and $L = 1000$ nm (solid curves) and different δ-dopings obtained with FV simulations.

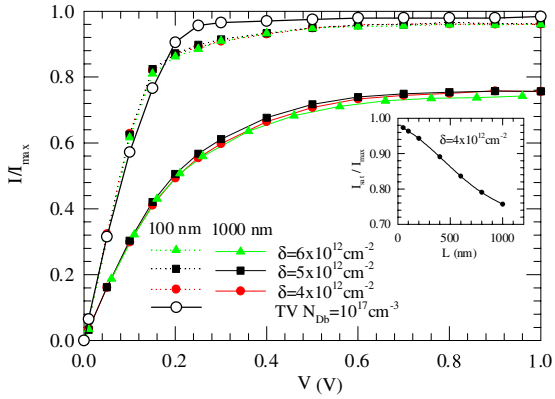

Figure 4. Normalized current density versus applied voltage for the non-recessed channels with lengths of 100 nm (dotted curves) and 1000 nm (solid curves) and different δ-dopings. Also the values obtained from TV simulations with $N_{Db} = 10^{17}$ cm^{-3} and $L = 100$ nm are shown. The inset shows the normalized saturation current as a function of the channel length for $\delta = 4 \times 10^{12}$ cm^{-2}.

values around 10 000 cm^2 V^{-1} s^{-1} measured experimentally. We have checked that this discrepancy is due to remote impurity scattering (that is not included in the MC model), since the experimental mobility of the channel is improved when a thicker spacer layer is grown, reaching around 14 000 cm^2 V^{-1} s^{-1}, in good agreement with the MC values. This layer structure will be used for the fabrication of the TBJs and diodes we will present later.

The simulated I–V characteristics of the channels (considering the whole layer structure using a FV simulation), consisting in a sample of length L between two ohmic contacts, are shown in figure 3 for $L = 1000$ and 100 nm. Depending on L, the diffusive or ballistic transport can be monitored, from the point of view of the MC simulation, by means of the number of scattering processes the electrons overcome while crossing the sample. However, transport will never be completely ballistic since, even for very short L, electrons will always overcome a few scattering mechanisms. We will show some other features that can give us information about how ballistic the transport inside the channels is, ranging from diffusive (for the channel with $L = 1000$ nm) to quasi-ballistic ($L = 100$ nm). One of these indicators is the ratio between the saturation current, I_s, and the total current injected by the contacts, I_{max}. In the case of completely ballistic transport $I_s = I_{max}$ since every electron injected by the cathode arrives to the anode (for high enough biasing). When scattering mechanisms appear, some carriers return to the anode, making the ratio I_s/I_{max} lower than unity. In figure 4 I/I_{max} is represented as a function of the applied voltage, showing that I_s/I_{max} increases when reducing L due to the lower amount of scattering mechanisms. The value of I_s/I_{max} as a function of L for the structure with $\delta = 4 \times 10^{12}$ cm^{-2} is plotted in the inset of figure 4 showing that for $L < 200$ nm I_s/I_{max} exceeds 95% and electron transport can be considered as quasi-ballistic. We have to note that the results plotted in figure 4 correspond to non-recessed channels (including the cap layer). In the case of recessed channels, impurity scattering in the cap layer is prevented and the ratio I/I_{max} is increased, but only for the long channels. The values of I/I_{max} for the 100 nm long non-recessed and recessed channels overlap, since the mean free path associated with ionized impurity scattering is longer than the length of the structures. Therefore, the recessed technology will be useful for improving the ballistic transport only when the length of the channels goes near the ballistic/diffusive limit (around 200 nm).

The simulation of the ballistic channels can also be made with TV simulations, considering a background doping, N_{Db}, with no impurity scattering. In figure 4 the I–V curve obtained with this model is compared with the correct FV simulations of the recess channels. It can be appreciated that setting the background charge to a value $N_{Db} = 10^{17}$ cm^{-3} and considering injecting contacts with $N_c = 4 \times 10^{17}$ cm^{-3} [5], TV simulations provide an acceptable modelling of the ballistic channels behaviour (both recessed and non-recessed). These values will therefore be used in the following TV simulations.

Other useful indicators of ballistic transport inside the devices are the profiles of electron energy and velocity in the channel (figure 5). For the short channels the absence of scattering mechanisms makes the electron mean energy increase with the same slope as the electric potential, figure 5(b), and an important velocity overshoot is observed, figure 5(d), both features showing the quasi-ballistic character of the transport. In contrast, diffusive transport is detected in the long structures since inelastic scattering makes the electron energy relax and not gain the whole potential energy contribution from the electric field, figure 5(a), also leading to a constant saturated velocity throughout the whole channel, figure 5(c).

3.2. T-branch junctions (TBJs)

As a first example of devices that benefit from ballistic transport we analyse the main features of a TBJ. The experimental measurements of the potential at the bottom of the central branch of a TBJ, V_C, when the left and right ones are biased

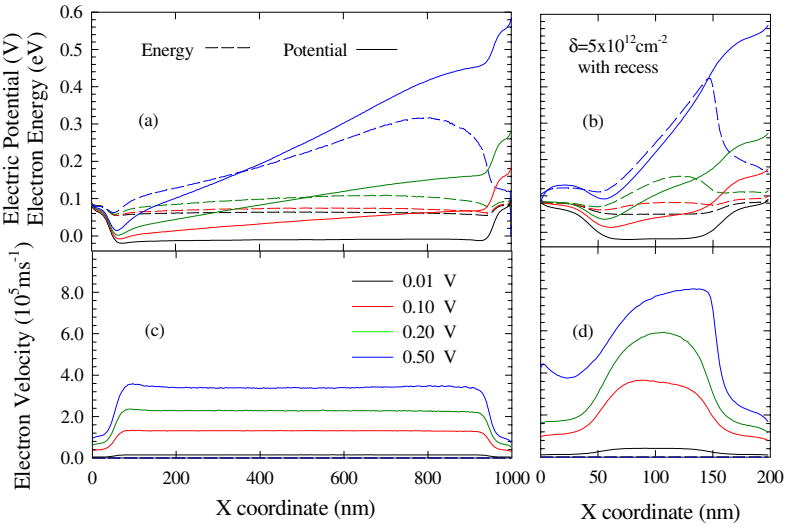

Figure 5. (a) and (b) Electric potential and electron energy and (c) and (d) electron velocity in the channel of the recessed structures with $\delta = 5 \times 10^{12}$ cm^{-2} and total lengths of (a) and (c) 1000 nm, and (b) and (d) 100 nm (a 50 nm non-recessed region is present near both contacts).

in push–pull fashion, $V = V_L = -V_R$ are presented in [1]. In figure 6 we show the values of V_C obtained with TV-MC simulations of a symmetric TBJ whose branches have a width of $W = 20$ nm and a length of 67 nm. They qualitatively reproduce the experimental results of [1], thus also supporting the validity of our TV-MC model. As seen in figure 6, the values of V_C depend on the amount of surface charge, since it controls the intensity of the space charge effects (the amplitude of the potential minimum). The effect of the surface charge is similar to that observed in [1] by changing the potential of a top gate contact, both affecting the Fermi level pinning and the electron concentration inside the TBJ. Consequently, the larger is the surface charge the lower is the current flowing through the horizontal branches, figure 6(b). The correct values of the background doping and surface charge density to be used in the TV-MC simulation will have to be further adjusted taking as a base the experimental measurements of channels with different length and width.

The negative values of V_C are related to space charge effects originated by the joint action of the surface charge at the semiconductor–air interfaces, the background positive fixed charge N_{Db} and the charge injected by contacts. The surface charge lowers the electric potential when moving away from the contacts provoking the progressive depletion of the channel, thus leading to the typical minimum of potential and concentration in the middle of the structure, figure 7, characteristic of space-charge-limited conditions [5]. When the TBJ is biased, the concentration shows an asymmetric shape (higher near the negative electrode due to the electron ballistic motion) leading to a shift of the potential minimum towards the negative electrode. As a consequence, the potential at the centre of the longitudinal channel is always negative (increasing with larger V) and propagates to the bottom of the vertical branch (inset of figure 7(b)), thus leading to the characteristic bell-shaped values of V_C. As stated in [6], this property of the TBJs can be very useful from a practical point of view, since it can be exploited to perform logical operations. It is also important to remark that this is a purely classical effect

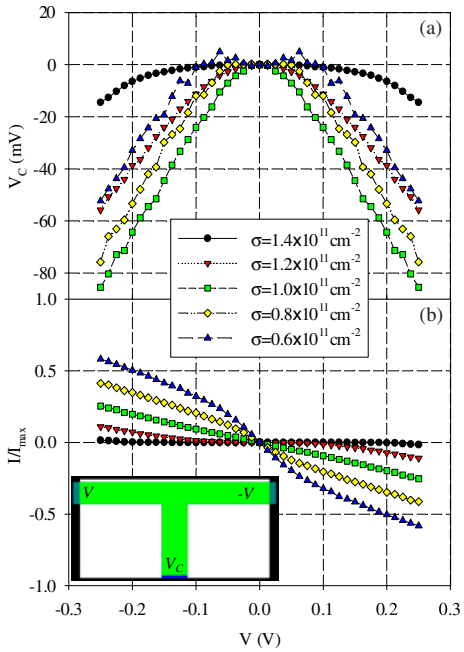

Figure 6. (a) Electric potential at the bottom of the central branch (open circuited) of the TBJ and (b) normalized horizontal current when biasing the left and right contacts in push–pull fashion ($V = V_L = -V_R$) for different values of the lateral surface charge. The inset shows the geometry of the TBJ.

related to ballistic transport and a quantum description of the system, as made in [6], would not be necessary to explain these results.

In figure 6 we can also observe that the negative values of the V_C versus V curve reach a maximum for an intermediate value of σ, just when the lateral depletion length, L_d, coincides with the width of the channel (for $N_{Db} = 10^{17}$ cm^{-3} and $\sigma = 1.0 \times 10^{11}$ cm^{-2}, assuming total depletion one has $L_d = \sigma / N_{Db} = 10$ nm, so that the theoretical effective width of the channel, $W_{eff} = W - 2L_d$, becomes 0). This happens

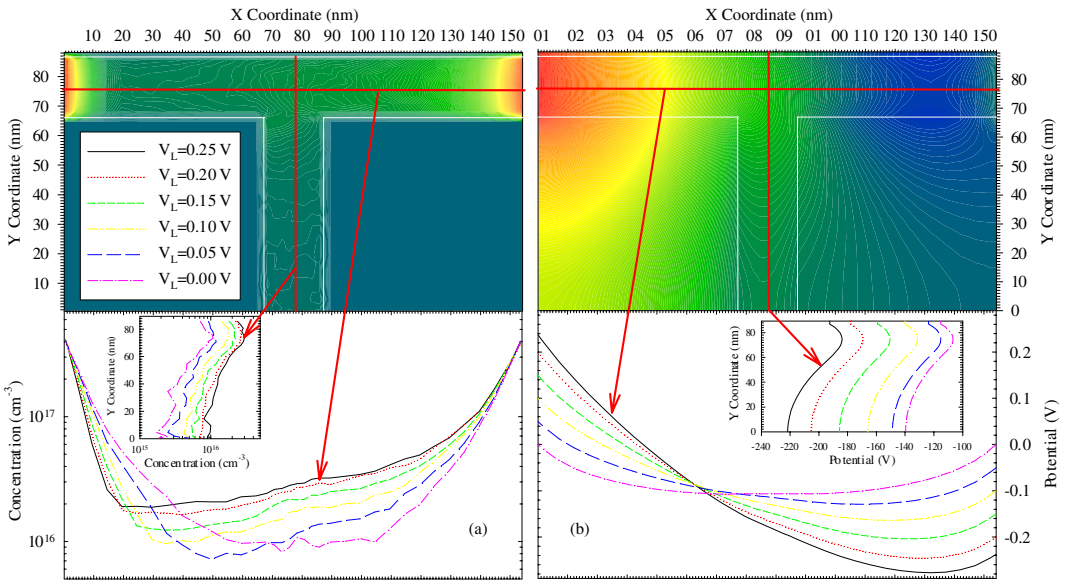

Figure 7. (a) Electron concentration and (b) electric potential profiles (horizontal and vertical) of the TBJ for different bias conditions and 2D charts for $V = V_L = -V_R = 0.25$ V.

since under these conditions the maximum non-uniformity of the electron concentration is obtained. The negative values of V_C are reduced both when the surface charge is larger or smaller than $\sigma = 1.0 \times 10^{11}$ cm^{-2}, since in the first case the channel tends to be depleted and in the second the weak surface charge lets the electron concentration be equal to N_{Db} (with practically constant values along the whole channel).

As an example of a prospective practical device using a TBJ, we will analyse the performance of a MUX/DEMUX implemented by means of a gate electrode deposited on the top of the TBJ. Depending on the biasing of the gate electrode, V_G, the electron flux coming form the source (left branch) will be deflected either to the right, or to the centre drain electrode (which are equally biased $V_{DR} = V_{DC}$). In figure 8 the current of both drain electrodes is represented versus V_G for $V_{DR} = V_{DC} = 0.5$ V. In the figure we also sketch the geometry of the simulated MUX/DEMUX with 40 nm wide branches, which has been slightly modified with respect to the simple TBJ to improve its switching performance. The situation of the gate electrode in this simplified TV simulation (using a surface charge density of 0.1×10^{12} cm^{-2}) is also shown. In order to demonstrate the ultra-high-frequency operation of this device, figures 9(b) and (c) show the current flowing through the right and central branches, respectively, when a square wave (+0.75/−0.75 V) of 1 THz frequency, figure 9(a), is applied to the gate electrode. Even if the geometry of the simulated device must be further optimized and does not exactly correspond to the 3D geometry of the real device, we can observe the ability of the device to perform the MUX/DEMUX function at THz frequency within acceptable limits. Moreover, we have to note that the intrinsic high-frequency capabilities of the device will be deteriorated due to the extrinsic contact resistances and capacitances, and therefore, strong efforts (both at technological and design levels) must be made to minimize their effect.

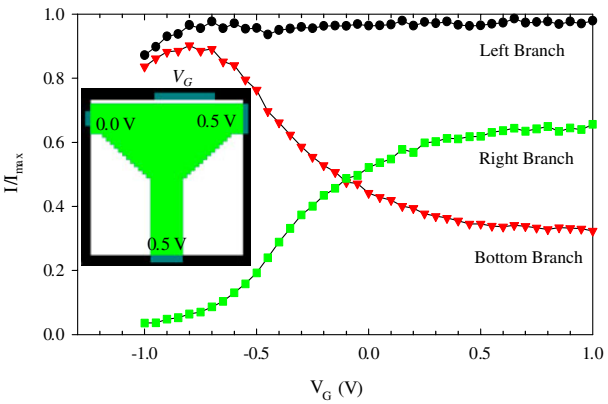

Figure 8. Normalized current density in the left, central and right branches of the MUX/DEMUX as a function of the gate voltage for $V_{DR} = V_{DC} = 0.5$ V. The inset shows the geometry of the simulated device.

3.3. Ballistic rectifier

Another practical device that can be envisaged taking advantage of electron ballistic transport is a ballistic rectifying diode. The I–V characteristics of the diode with the sketched geometry are plotted in figure 10 ($\sigma = 1.0 \times 10^{11}$ cm^{-2}). Even if a proper rectifying behaviour is not achieved (the inverse current is quite high), it can be appreciated that the I–V curve shows a different slope for direct and reverse biasings, thus becoming a non-linear device. This non-linear behaviour is a result of ballistic transport since a similar long diffusive diode would behave as a simple resistance. The inset of figure 10 shows the time-dependent current when applying a switching bias (between +0.25 and −0.25 V) at 1 THz frequency, demonstrating the capability of this diode for THz operation (even if further modifications must be made to achieve good rectifying characteristics). The importance of space charge for the 'rectifying' characteristics is evidenced in figure 11 by the asymmetric electron distribution observed for direct and reverse bias, which leads to a non-linear I–V dependence.

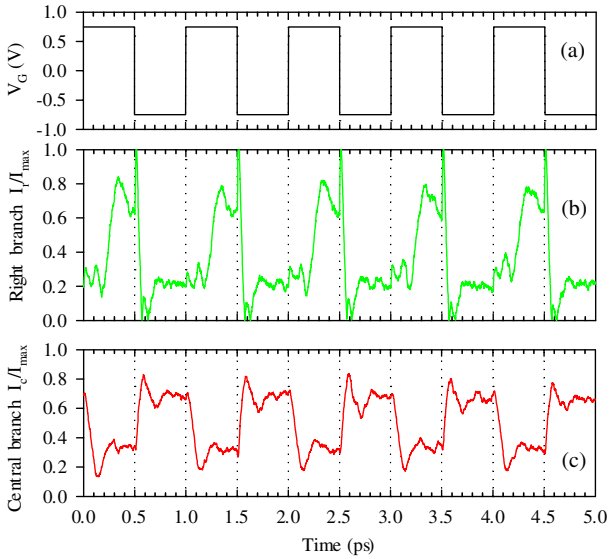

Figure 9. (a) 1 THz square signal applied to the gate and normalized time-dependent current in the (b) right and (c) central branches of the MUX/DEMUX.

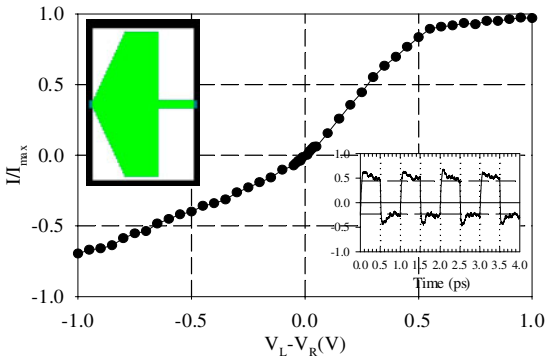

Figure 10. Current flowing through the ballistic rectifier as a function of the biasing. The insets show the time-dependent current when biasing with a square signal (+0.25/−0.25 V) of 1 THz frequency. The geometry of the diode is also shown (120 nm long and widths of the narrow and wide regions of 20 and 220 nm, respectively).

In the case of reverse biasing ($V_L = 0V, V_R > 0V$), the electron concentration decreases in the narrow part of the device since it is not easy for the electrons moving towards the right to enter in such a narrow channel. Therefore, the total resistance of the diode is much increased with respect to the equilibrium value (the narrow region is the most resistive one). In contrast, when applying a direct bias, the electron concentration increases, thus decreasing the total resistance and providing a non-linear behaviour for this diode.

4. Conclusions

By means of a semi-classical MC simulation, evidence of quasi-ballistic transport at room temperature is found in 100 nm long InGaAs channels. Experimental Hall effect measurements have been used to calibrate the model. Also, the qualitative agreement of our results with measurements of the potential at the bottom of the central branch of TBJ, V_C, supports the validity of our method. The origin of the negative values of V_C is in the presence of a potential minimum in the centre of the TBJ associated with space charge (created by the surface charges), and is not related to any quantum effect. The possibility of taking advantage of ballistic transport for fabricating practical devices working at THz rate has been demonstrated. As an example, preliminary results of a MUX/DEMUX fabricated taking as a base a TBJ, and a ballistic rectifying diode have been presented.

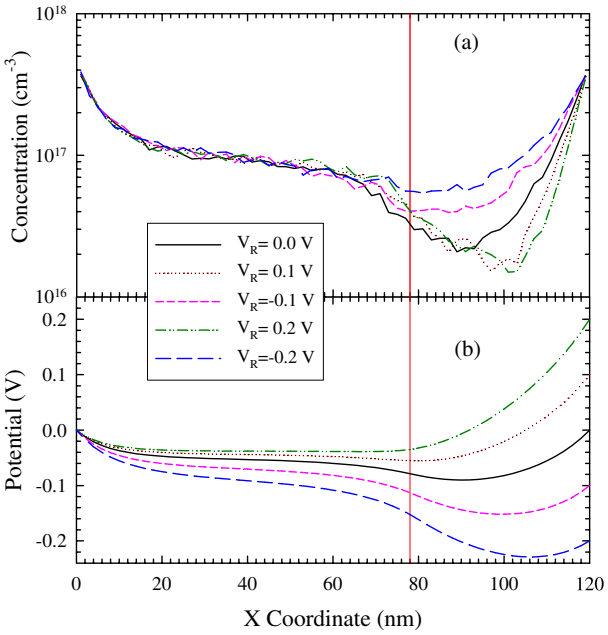

Figure 11. Profiles of (a) concentration and (b) electric potential in the ballistic rectifier for different direct ($V_R < 0V$) and reverse bias ($V_R > 0V$), with $V_L = 0V$. The vertical line shows the situation of the narrow/wide channel transition.

Acknowledgments

This work has been partially supported by the European Commission through the NANOTERA project IST-2001-32517, by the Dirección General de Investigación (Ministerio de Ciencia y Tecnología) and FEDER through the project TIC2001-1754 and by the Consejería de Cultura de la Junta de Castilla y León through the project SA057/02.

References

[1] Shorubalko I, Xu H Q, Maximov I, Omling P, Samuelson L and Seifert W 2001 *Appl. Phys. Lett.* **79** 1384
[2] Mateos J, González T, Pardo D, Hoel V and Cappy A 2000 Improved Monte Carlo algorithm for the simulation of δ-doped AlInAs/GaInAs HEMTs *IEEE Trans. Electron Devices* **47** 250
[3] Mateos J, González T, Pardo D, Hoel V and Cappy A 1999 Effect of the T-gate on the performance of recessed HEMTs. A Monte Carlo analysis *Semicond. Sci. Technol.* **14** 864
[4] Mateos J, González T, Pardo D, Hoel V and Cappy A 2000 Monte Carlo simulator for the design optimization of low-noise HEMTs *IEEE Trans. Electron Devices* **47** 1950
[5] González T, Bulashenko O M, Mateos J, Pardo D and Reggiani L 1997 *Phys. Rev.* B **56** 6424
[6] Xu H Q 2001 Electrical properties of three-terminal ballistic junctions *Appl. Phys. Lett.* **78** 2064